Photothermal analysis of therapeutic nanoparticles

Author: Gori Camps Tomàs
Facultat de Física, Universitat de Barcelona, Diagonal 645, 08028 Barcelona, Spain.

Advisor: J. Marcos Fernández-Pradas

Abstract: Nanoparticle-mediated photothermal therapy is a well documented, highly selective cancer treatment strategy, both as a standalone and complementary therapy. The efficiency of light-to-heat transduction serves as a benchmark parameter when comparing different nanoparticles. This work aims to design an experimental setup for efficiency calculation through the temperature curve. An additional equation for surrounding temperature is added to more accurately interpret the experimental data. Introduction of exhaust fans minimizes ambient temperature variation as suggested by the model. Continuous-wave laser irradiation at 1064 nm and 0.2-1.0 W on an aqueous solution of Prussian blue nanoparticles with an iron oxide core is used to heat the sample and stopped after reaching a stable equilibrium temperature. The obtained value of the efficiency is $\eta = 0.24 \pm 0.03$. Overall, the experimental setup with forced heat extraction is useful to obtain temperature curves for efficiency calculation. Furthermore, the used nanoparticles are not ideal for photothermal therapy due to low efficiency.

I. INTRODUCTION

The term cancer refers to a group of diseases involving abnormal growth of cell tissue, potentially invading other areas of the body. Because of the high risk and high mortality rate, efforts are underway to develop more accurate diagnostic techniques and effective therapies. Traditionally, the most prominent treatments have been chemotherapy, radiotherapy, immunotherapy and surgery. Serious side effects are associated with all the above treatment options. Thus, current research focuses on finding alternative or complementary therapy that helps reduce unwanted harmful byproducts.

A temperature increase above a certain threshold induces cell death. This phenomenon is known as thermoablation. However, a temperature increase below the thermoablation threshold may still have therapeutic benefits while limiting damage to noncancerous tissue[1]. The latter is known as hyperthermia (HT). HT depends not only on the maximum temperature reached but also on exposure time, type of tissue and other factors. HT aims to produce a minimum increase in temperature such that the induced biochemical changes in the tissue benefit other therapy options. In this regard, HT is usually a complementary treatment. Unfortunately, traditional methods for increasing temperature are not specific enough, resulting in heat-induced side effects in noncancerous tissue.

A more promising approach to HT is the use of photothermal properties of some nanoparticles (NPs). Photothermal Therapy (PTT) is the use of NPs to transform light energy into heat to increase the temperature of the surroundings and induce cell death. The main advantage of NP-mediated HT is the versatility of NP synthesis: custom nanoparticles can be engineered to meet desired needs. For example, NPs can be designed to target tumours through specific receptors, contributing to a higher tumour-to-cell accumulation ratio. Moreover, NPs can be visualized *in vivo* with certain imaging technologies, which may allow tumour detection and treatment with the same NPs[2].

The main challenge in this type of therapy is finding a biocompatible NP with high enough efficiency to selectively induce a temperature increase in cancer cells within the skin threshold power density. Light in the NIR-I window (650-950 nm) is commonly used in PTT applications[3]. However, light in the NIR-II window (1000-1350 nm) has been shown to have a deeper tissue penetration[4] (specially in the 1000-1100 nm range). Furthermore, a 1064 nm laser has a maximal permissible exposure of $1\,\mathrm{W\,cm^{-2}}$ according to the American National Standards Institute, whereas a 801 nm laser's maximal permissible exposure is $0.33\,\mathrm{W\,cm^{-2}}$[5].

The general guideline for the present work is based on D. Keith Roper's work in *Microscale Heat Transfer Transduced by Surface Plasmon Resonant Gold Nanoparticles*[6]. In the presented paper, efficiency is proposed as benchmark parameter for usefulness of NPs for PTT[6]. The main objectives of this study are two-fold. Most importantly, to design a suitable experimental setup to obtain the NPs' efficiency through their temperature curve. Secondly, to test the effectiveness of a type of NPs for PTT using continuous-wave irradiation with light in the NIR-II window, according to the efficiency parameter mentioned above.

Nanoparticles used in this work are designed with iron oxide as core and a Prussian blue envelope (PBMNP). The iron core is magnetic and allows both NP direction through magnetic fields and visualization *in vivo*. The Prussian blue envelope is the light-absorbing agent.

II. MATHEMATICAL MODEL

Here, the equations behind the process, which will guide the design of the experiment, are described.

A. Derivation

A two-part system is considered: the first component is the aqueous solution of nanoparticles and the second one are the surroundings (polystyrene container and surrounding air). Each component's temperature is assumed to be homogeneous. The variation in temperature in the sample must be proportional to the heat input of the laser minus the heat transfer to the surroundings, with the inverse of the heat capacity being the proportionality constant. Similarly, ambient temperature is proportional to the heat input from the outward heat flow of the sample minus the heat loss to the laboratory. The laboratory temperature is assumed to be constant. Let h and h_s be the heat transfer coefficients of the sample and surroundings, respectively. Let A and A_s be the total cross-section perpendicular to heat transfer in the sample and surroundings, respectively. For simplicity of the equations, consider $G = h \cdot A$ and $G_s = h_s \cdot A_s$, with SI units of $\mathrm{W\,K^{-1}}$. Let k and k_s be the total heat capacities of each component, with SI units of $\mathrm{J\,K^{-1}}$. Finally, let Q_{in} be the heat per unit time introduced by the laser, with SI units of W. Let $t = 0$ the time the laser is turned on and let t_0 be the time the laser is turned off. Thus, the source term Q_{in} is zero from t_0 onward. Temperatures are shifted by the laboratory temperature for ease of solution: scaled temperatures $u = T - T_{LAB}$ and $u_s = T_s - T_{LAB}$ are defined. With all the above, the equations of the model can be written as follows:

$$\begin{cases} \dot{u} = -\dfrac{G}{k}\left(u - u_s\right) + \dfrac{Q_{in}}{k} \\ \dot{u}_s = \dfrac{G}{k_s}\left(u - u_s\right) - \dfrac{G_s}{k_s}u_s \\ u(t=0) = 0 \\ u_s(t=0) = 0 \end{cases} \tag{1}$$

Notice that the right-hand side of the first equation is not continuous. Indeed, the source term Q_{in} is abruptly made zero at $t = t_0$. A solution to the Cauchy problem is given by the continuous concatenation of the respective solutions in $t < t_0$ and $t > t_0$. The constants of the latter are determined using the requirement of continuity. The constant $\tau = k/G$ is defined. Clearly, this constant has units of time, and will be referred to as the time constant.

B. Solution

To solve the equations, parameters G, G_s, k and k_s are assumed to be time-independent. The ideal case corresponds to a very large k_s, indicating that the system's surroundings act as a thermal font. In this particular situation, the second equation in system (1) together with the initial condition simply yields $u_s = 0$, that is, ambient temperature is constant and equal to T_{LAB}. A zeroth-order solution in the sense of Section II A at $1/k_s = 0$ is obtained in equation (2).

$$u\left(t;0\right) = \begin{cases} \frac{Q_{in}}{G} \cdot \left(1 - e^{-\frac{G}{k}t}\right) & \left(t \le t_0\right) \\ \frac{Q_{in}}{G}\left(1 - e^{-\frac{G}{k}t_0}\right) \cdot e^{-\frac{G}{k}\left(t - t_0\right)} & \left(t_0 \le t\right) \end{cases} \tag{2}$$

Solution (2) is the same as in the reference article[6], with two slight modifications. First, the cooling and heating branches have been concatenated to fit the whole data set at the same time. This way, a single value of the fitted parameter is obtained, as opposed to one for each branch, which may not coincide. Second, from the steady-state of equation (1), it is seen that Q_{in}/G is the maximum value of u, u_{MAX}. Either parameter may be used to express the solution.

To better capture the physical nature of the process, a solution for the case $1/k_s \neq 0$ is desirable. The solution for a linear system with a constant matrix can be analytically found. The cooling branch solution, which corresponds to the homogeneous system, is presented in equation (3). For simplicity's sake, when only the cooling is considered, it is assumed that $t_0 = 0$. The heating solution can be obtained by variation of constants, but will not be considered at the moment.

$$\begin{aligned} u\left(t;\frac{1}{k_s}\right) = \exp\left\{-\frac{t}{2}\cdot\left(\frac{G}{k} + \frac{G+G_s}{k_s}\right)\right\}\cdot \\ \left[F(G,G_s,k,k_s)\cdot e^{-\frac{t}{2}\xi} + H(G,G_s,k,k_s)\cdot e^{\frac{t}{2}\xi}\right] \end{aligned} \tag{3}$$

Functions F and H depend on the parameters, but are time-independent. Their limits when k_s is arbitrarily large are u_{MAX} and 0, respectively, so that the ideal solution can be re-obtained. Moreover, $F + H = u_{MAX}$. Additionally, ξ is the following root:

$$\xi = \sqrt{\left(\frac{G}{k}\right)^2 + \left(\frac{G+G_s}{k_s}\right)^2 + \frac{2GG_s + 6G^2}{kk_s}} \tag{4}$$

The general solution can be thought of as an exponential whose amplitude is dependent on time through two exponential functions with opposite arguments and complementary amplitudes. This partial expression may be used to heuristically emphasise an important point. If the solution is expanded in Taylor series near $1/k_s = 0$, ignoring for now the variation of F and H:

$$u(t) \simeq \left[\left(1 - \frac{G+G_s}{2k_s}t\right)\cdot\left(1 - \frac{G_s+3G}{2k_s}t\right)\right]e^{-\frac{G}{k}t} \tag{5}$$

The curve is closer to the ideal solution when the time is small compared to $(G+G_s)/(2k_s)$. Thus, it seems that the time constant in an experiment with $1/k_s \neq 0$ could be obtained fitting the start of the cooling to solution (2).

III. EXPERIMENTAL SECTION

A. Experimental Setup

Nanoparticle solution is poured in a polystyrene container. Continuous-wave Laser (Baasel, LBi6000, 60W,

$\lambda = 1064\,\text{nm}$, a diaphragm is placed in the laser resonant cavity, effectively lowering the maximum power and guaranteeing a Gaussian profile of the beam) radiation is reflected in a mirror aimed at the sample. A thermopile is set behind the sample container to measure the radiation that has not been absorbed. The thermopile is connected to a multimeter. Temperature is measured with two thermocouples. The first one is completely submerged in the NP solution, close to the container wall and away from the laser beam to avoid direct exposure. The second thermocouple is placed outside the container and in contact with the wall behind the first thermocouple. After a first set of experiments, two exhaust fans are placed on the sides of the sample container, both connected to a generator at 12 V. The objective is to have a better control over the surroundings' temperature. A temperature-controlled breadboard is set up under the sample, allowing for temperature regulation. This breadboard is unused in the experiments with the extraction fans. A schematic view of the setup (FIG. 1) and a picture of the complete system with the fans (FIG. 2) are presented.

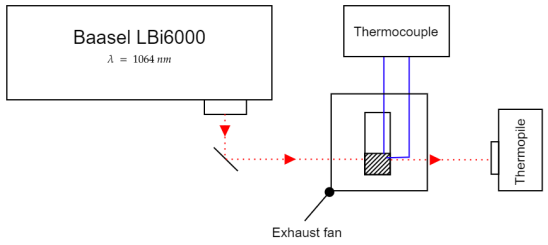

FIG. 1: Scheme of the experimental setup. The exhaust fans are drawn as a square around the sample. The laser is represented by a red dotted line. The solution is represented as a dashed area inside the container.

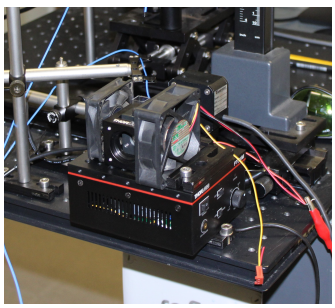

FIG. 2: Photography of the setup described in FIG.1.

B. Experimental Procedure

An aqueous solution of NPs with iron oxide core and a Prussian blue envelope (PBMNPs) was supplied by the "Col·loids" group of the *Dept. Farmàcia i Tecnologia Farmacèutica i Fisicoquímica*. Sample solutions with 100%, 50%, 25% and 12.5% volume concentrations of the original were prepared in separate containers. Heating experiments with different volumes revealed that 0.5 mL allows homogeneous heating of the majority of the sample while being manageable.

For each experiment, the laser power was set and then directly measured with the thermopile for greater precision. After this measurement, the sample was mounted in the supporting structure. The mirror was adjusted so the beam aimed directly below the meniscus of the solution in the container, low enough that the laser beam was entirely submerged even after slight evaporation occurred. Then, the thermocouples were placed. After the system reached thermal equilibrium, the laser was turned on but blocked so that no radiation was going to the sample. This procedure contributes to laser stabilization and avoids unnecessary oscillations in power. After approximately half a minute, when the laser was the most stable, the opaque material used to block the beam was removed. Beam power after absorption in the sample was measured, again, using the thermopile. Laser incidence stopped when the measured temperature had remained constant for around three minutes. Afterwards, the sample was left to cool to ambient temperature. Data recording stopped when the temperature of the sample and the ambient were equal to the laboratory temperature.

Heat absorbed by the sample was calculated as the incident power minus the outgoing power. The effects of the container were introduced through Fresnel equations. The refractive index of the container was measured to be 1.65 ± 0.05. Incidence is assumed to be normal so that transmission coefficients at the polystyrene-sample and sample-polystyrene interfaces are easy to calculate. Let these values be T and T' respectively. Then if I and I' are the input and outgoing intensities, respectively:

$$Q_{in} = T \cdot T' \cdot I - \frac{I'}{T \cdot T'} \tag{6}$$

Two types of fittings were made, both using the *Curve Fitting Tool* from MATLAB[7]. On the one hand, equation (2) was fitted to the experimental curve via the custom equation option. On the other hand, the logarithm of the first 220 s of the cooling process was fitted to a line.

IV. RESULTS AND DISCUSSION

A typical plot of the normalised temperature u/u_{MAX} against time for an experiment performed with the heated breadboard but without the heat extraction fans is shown in FIG. 3. Continuous-wave laser irradiation at (0.9 ± 0.1) W is applied. Temperature increased from ambient temperature $T_{LAB} = 31.3\,^{\circ}\text{C}$ to a maximum temperature $T_{MAX} = 54.7\,^{\circ}\text{C}$ after 600 s (70.8% increase) while ambient temperature experimented a 24.5% increase. The fit in FIG. 3 is done using the zeroth order solution (2). The fitting parameter is the time constant

described in Section II A. Similarly, FIG. 4 is the fit of the start of the cooling.

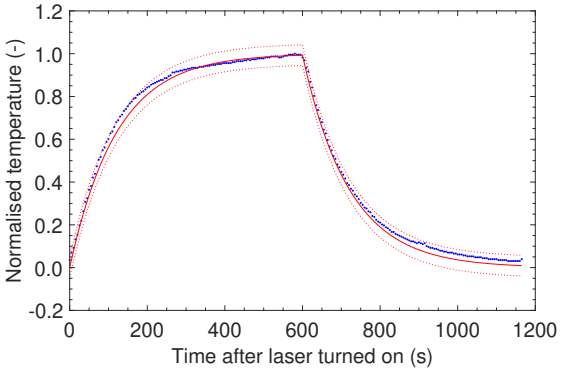

FIG. 3: Sample lin-lin plot of dimensionless temperature vs time. Experiment performed without fans, with 100% volume concentration and input power (0.9 ± 0.1) W. Cooling start time is $t_0 = 600$ s. The zeroth order model is used. The regression coefficient is $R^2 = 0.996$. Dotted line corresponds to 95% confidence bound.

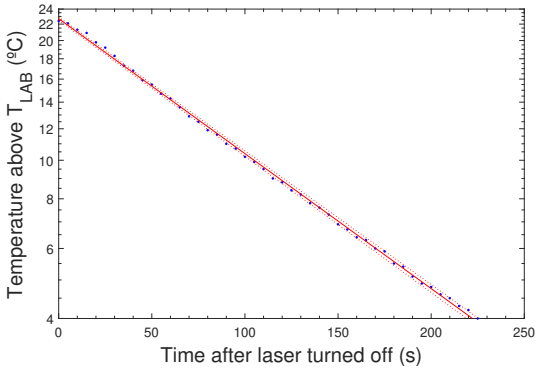

FIG. 4: Sample lin-log plot of dimensionless temperature vs time (100% concentration, no fans, (0.9 ± 0.1) W input). The first 220 s of the cooling are fitted to the ideal model. The regression coefficient is $R^2 = 0.9991$. Dotted line corresponds to 95% confidence bound.

An average time constant $\tau_s = (137 \pm 4)$ s $(N = 8)$ is obtained for the experimental setup without the fans and the zeroth order model. An average time constant $\tau_s = (137 \pm 4)$ s $(N = 8)$ is obtained for the same setup but fitting only the start of the cooling process.

A typical plot of the normalised temperature as a function of time in the exhaust fan setup is shown in FIG. 5. The sample is brought to thermal equilibrium with the surroundings for 30 s. Continuous-wave laser irradiation at (0.7 ± 0.1) W is applied. Temperature increased from ambient temperature $T_{LAB} = 18.7\,^{\circ}$C to a maximum temperature $T_{MAX} = 27.5\,^{\circ}$C after 510 s (46.5% increase) while ambient temperature experimented a 4.2% increase. Fitting of the first part of the cooling process is shown in FIG. 6.

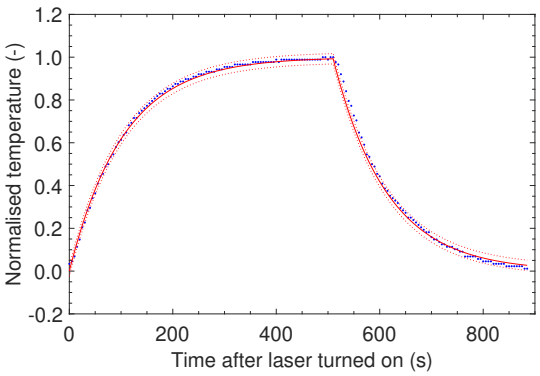

FIG. 5: Sample lin-lin plot of dimensionless temperature vs time. Experiment performed with fans, 25% volume concentration and input power (0.7 ± 0.1) W. This fit is performed using the zeroth order model. Cooling start time is $t_0 = 500$ s. The regression coefficient is $R^2 = 0.9992$.

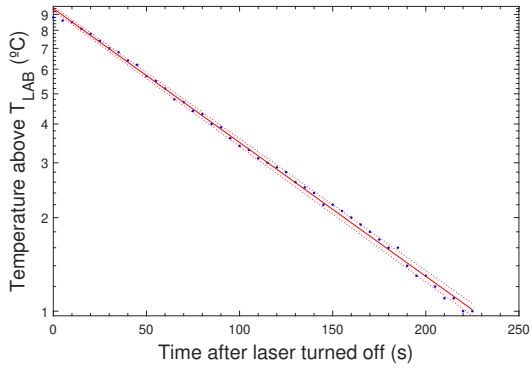

FIG. 6: Sample lin-log plot of dimensionless temperature vs time. Experiment performed with fans, with 25% volume concentration and input power (0.7 ± 0.1) W. The beginning of the cooling is fitted to the zeroth order model. The regression coefficient is $R^2 = 0.9992$.

An average time constant $\tau_s = (104 \pm 4)$ s $(N = 12)$ is obtained for the this experimental setup using the whole data set. An average time constant $\tau_s = (101 \pm 2)$ s $(N = 12)$ is obtained for the same experimental setup and only the start of the cooling process.

Comparisson of the two sets of experiments reveals that neglecting the terms with k_s in the experiments without fans results in an overestimation of the time constant. Controlling surrounding temperature is, then, preferable to using the zeroth order (ideal) solution only in the beginning of the cooling.

The efficiency of transducing incident light to heat is measured using equation (7) and computed only for the experiments with forced heat extraction:

$$\eta = \frac{G(T_{MAX} - T_{LAB}) - Q_0}{Q_{in}} = \frac{G \cdot u_{MAX} - Q_0}{Q_{in}} \qquad (7)$$

The heat absorbed by water, Q_0, was determined with the same experimental setup and deionized water as

the sample. The obtained values at (0.25 ± 0.05) W, (0.75 ± 0.05) W and (0.99 ± 0.05) W are, respectively, (0.06 ± 0.01) W, (0.11 ± 0.01) W and (0.17 ± 0.01) W. The value of G is determined from the time constant as $G = k/\tau$, where k is approximated as the heat capacity of the 0.5 mL of water (thus neglecting the contribution of the nanoparticles). The result is $\eta = 0.24 \pm 0.03$. Relative uncertainty is 12.5%.

In light of this results, the fans have proven useful in reducing variation in ambient temperature from an inconsistent 5 %-20 % change to being consistently below 5%. As expected from equation (3), the fit is more accurate near the beginning of the cooling. In the experiments without the fans, a greater deviation of the model is observed at the end of the cooling process. After the introduction of the heat extraction system, this deviation is corrected significantly. Fitting of the whole data set is consistent with heating of the cooling in both setups. Finally, instabilities in laser power have limited the number of experiments that were usable to perform the fittings.

1. *Therapeutic considerations*

The total area of the spot has been measured to be $A = (10.2 \pm 0.1)\,\mathrm{mm}^2$. A sufficiently large temperature increase need be produced with a low enough power so that surrounding tissue is not damaged. Hyperthermia is usually assigned a range of 40 °C-50 °C, with temperatures above 50 °C being considered thermoablation[3].

With the maximum concentration available, a thermoablation inducing temperature increase of 14 °C, requires an input power of (0.78 ± 0.05) W, which corresponds to a power density of $(7.6 \pm 0.5)\,\mathrm{W\,cm^{-2}}$, above the limit of $1\,\mathrm{W\,cm^{-2}}$[5]. In the same way, for a temperature increase of 5 °C at maximum concentration a power input of (0.24 ± 0.05) W is required, leading to a power density of 2.4 ± 0.5, still above the threshold. Thus, the nanoparticles do not seem suitable for PTT in the NIR-II window. The peak of absorption of Prussian blue occurs at 735 nm[8], thus the efficiency of PBMNPs should be higher at the NIR-I window.

V. CONCLUSIONS

Efficiency calculation is essential in comparing NP candidates for PTT. Control over the variation of temperature in the surroundings is important to ensure experiment reproducibility and accuracy. As seen, a constant ambient temperature simplifies the fitting by allowing the use of a more manageable equation. Moreover, in this situation, the whole data set can be fitted using a single curve, yielding a single value for the time constant. Crucially, when the surrounding temperature is not controlled, the time constant is not correctly measured. What's more, this incorrect measure of the time constant is not overcome by fitting only the start of the cooling, as proposed in the heuristic of Section II B.

With the designed experimental setup, it has been seen that the PBMNPs are not ideal for PTT in the NIR-II window. With such low efficiency, power densities above the skin tolerance threshold are needed to produce meaningful temperature increases. A higher efficiency could be achieved by using a laser with wavelength closer to the absorbance peak of Prussian blue, in the NIR-I window.

Limitations imposed by laser instability have negatively impacted the experiments. A more stable laser could improve experiment quality. We hope that with a more stable laser and this experimental setup, testing of NP efficiency will be much easier and further experiments with different types of NPs will be done to find better candidates for PTT.

Acknowledgments

I would like to thank my advisor J. Marcos Fernández for his continued support and patience and Dr. Pol Sopeña for helping me in the laboratory, as well as my family and friends.

[1] J.C. Peeken, P. Vaupel, *et al.*, "Integrating hyperthermia into modern radiation oncology: What evidence is necessary?", Front. Oncol. **7**, 132 (2017)

[2] Y. Liu, P. Bhattarai, *et al.*, "Photothermal therapy and photoacoustic imaging via nanotheranostics in fighting cancer", Chem. Soc. Rev. **48**, 2053-2108 (2019)

[3] P. Kaur, M.L. Aliru, *et al.*, "Hyperthermia using nanoparticles-promises and pitfalls", Int. J. Hyperthermia. **32**, 76-88 (2016)

[4] P.K. Upputuri, M. Pramanik, "Photoacoustic imaging in the second near-infrarated window: a review", J. Biomed. Opt., **24**, 1-20 (2019)

[5] ANSI Z136.1-2014, *American National Standard for safe use of lasers* (2014).

[6] D.K. Roper, W. Ahn, *et al.*, "Microscale heat tranfer transduced by surface plasmon resonant gold nanoparticles", J. Phys. Chem. C. **111**, 3636-3641 (2007)

[7] MATLAB, *R2020b* (The MathWorks Inc., 2020)

[8] M. Cheng, W. Peng, *et al.*, "In situ formation of photoresponsive Prussian blue for photoacoustic imaging and photothermal therapy of cancer", RSC. Adv. **7**, 18270-18276 (2017)